Phys. Status Solidi A **206**, No. 5, 796–802 (2009) / **DOI** 10.1002/pssa.200881407

physica status solidi a
www.pss-a.com
applications and materials science

Room temperature characterisation of InGaAlAs quantum well laser structures using electro-modulated reflectance and surface photovoltage spectroscopy

Natasha E. Fox[1], Tarun K. Sharma[2], Stephen J. Sweeney[1,3], and T. J. C. Hosea[*,1]

[1] Department of Physics, University of Surrey, Guildford, Surrey, GU2 7XH, UK
[2] On deputation from Raja Ramanna Centre for Advanced Technology, Indore, India
[3] Advanced Technology Institute, University of Surrey, Guildford, Surrey, GU2 7XH, UK

Received 3 July 2008, revised 24 November 2008, accepted 2 December 2008
Published online 17 March 2009

PACS 78.20.Ci, 78.30.Fs, 78.67.De, 85.60.Bt

[*] Corresponding author: e-mail j.hosea@surrey.ac.uk, Phone: + 44 1463 689412, Fax: +44 1483 686781

In this study, two tri-metal quaternary InGaAlAs quantum well (QW) laser structures grown on InP are compared to a conventional InGaAsP QW structure, also grown on InP, all designed to lase at 1.55 μm. Several spectroscopic methods are used to study the samples including surface photo-voltage (SPV) and electro-modulated reflectance (ER). In the tri-metal samples the ground- and two excited-state QW transitions are detectable in both types of spectroscopy. The SPV and ER give results in agreement to within a few meV of each other. By comparing the position of the measured QW transitions with those predicted theoretically, the conduction band offsets of the tri-metal samples can be determined and compared to that in the InGaAsP sample. It is found that the tri-metal samples have a much larger conduction band offset of ~66% compared to the ~40% in the InGaAsP sample.

1 Introduction 1.3 μm and 1.55 μm lasers are of great importance in the telecommunications industry since silica-based optical fibre has zero dispersion at 1.31 μm and minimum absorption at 1.55 μm [1]. A common approach to achieve lasing at such wavelengths is to use InGaAsP/InP which ranges in potential wavelength from 0.92 μm to 1.63 μm [2]. However, the tri-metal quaternary system InGaAlAs/InP offers greater versatility, ranging in wavelength from 0.85 μm to 1.63 μm, with the added advantage of a larger conduction band offset, which is expected to reduce device temperature sensitivity [2].

Surface photo-voltage (SPV) and electro-modulated reflectance (ER) are both useful spectroscopic techniques for giving detailed information on semiconductor band-structure at room temperature, without the need for cryogenics as is often necessary with photoluminescence measurements.

In ER, and its contactless counterpart photo-modulated reflectance (PR), the external perturbation of the quantum well (QW) confinement potential leads to a red shift of the interband transition energies, referred to as the quantum-confined Stark effect, which can reveal information on the QW ground state transition as well as higher order transitions. The modulated reflectance signal is defined as:

$$\frac{\Delta R}{R} = \frac{1}{R}\frac{\partial R}{\partial \varepsilon_1}\Delta\varepsilon_1 + \frac{1}{R}\frac{\partial R}{\partial \varepsilon_2}\Delta\varepsilon_2 , \qquad (1)$$

where ΔR is the modulated component of the reflectivity R, created by perturbing the internal field of the sample either with an applied AC field in ER, or a chopped pump laser in PR, and $\Delta\varepsilon_1$ and $\Delta\varepsilon_2$ are the respective real and imaginary parts of the sample modulated dielectric function. SPV can be thought of as a type of absorption spectroscopy [3]: for photons incident on the sample of energy greater than the bandgap, electrons and holes are generated which separate in the internal field. This induces a surface voltage which displays peaks whenever the photon energy is resonant with a QW transition.

2 Experimental details

2.1 Samples The two tri-metal device structures studied here (which we shall call samples 'A' and 'B') have nominally 1% compressively-strained quaternary InGaAlAs QWs, designed to emit at 1.55 μm, grown by MOCVD on InP substrates, with lattice matched InGaAlAs barriers. They have nominally identical layer structures as follows: (1) a lower n-type InP cladding region; (2) a 500 Å AlInAs carrier blocking layer; (3) a 1000 Å graded index InGaAlAs region; (4) a 200 Å InGaAlAs barrier matched to InP; (5) four 45 Å InAlGaAs QWs separated by barriers of 150 Å; (6) a 200 Å barrier; (7) a 1000 Å graded index InGaAlAs region; (8) a 500 Å AlInAs blocking layer; and (9) an upper p-type InP cladding. The only difference between samples is that in sample A the AlInAs blocking layers are intentionally doped (n- and p-type on respective sides of the active region, as per the InP cladding) whereas in sample B they are not. We were provided with the target bandgaps of the InGaAlAs barriers and graded-index regions which were ~992 meV, and from ~992 meV to ~1181 meV, respectively. The compositions were deduced subsequently, as explained later.

Here, these samples are compared to a "benchmark" sample based on the conventional InGaAsP/InP system, also designed to emit at 1.55 μm. This sample ('C') has a nominal composition of: (1) p-type cladding; 9 repeats of: (2) a 1.0% compressively-strained 65 Å $In_{0.80}Ga_{0.20}As_{0.74}P_{0.26}$ QW and (3) an 90 Å $In_{0.73}Ga_{0.27}As_{0.53}P_{0.47}$ barrier with nominal slight tensile strain of −0.2% and target bandgap of ~992 meV, and (4) an n-type InP cladding.

2.2 Method Initially, due to its simplicity, PR was attempted on all the samples, trying both 633 nm HeNe, and 1064 nm Nd:YAG, lasers as pumps. However, only the benchmark sample gave a measurable PR signal. This led us to investigate other techniques, i.e. the ER and SPV, in order to find a spectroscopic method that worked on all the samples. Each sample was mounted on a copper plate with conducting silver adhesive to act as the earth, whilst the front of the sample was touched in "soft-contact mode" [3] with a sheet of glass coated with indium tin oxide (ITO) to act as the top transparent electrode. The probe light for the ER and SPV measurements was provided by a 100 W quartz tungsten halogen lamp, and a monochromator, operated with a bandpass of 3 nm. In the ER measurements the sample was modulated at a frequency of 332 Hz, with typically an AC field of amplitude 1.31 V and a reverse DC bias of −1.31 V, with the reflected signal measured at an incidence angle of about 23°. A lock-in amplifier was used to measure the ΔR signal detected by an InGaAs detector. The SPV was measured in the standard way [4], with the sample at normal incidence, with a chopper (again at 332 Hz) in front of the monochromator output slit and the same instrumental bandpass. The modulated SPV was measured using the lock-in amplifier. The SPV signals were corrected later for the system response by measuring the light throughput using the InGaAs detector and normalising using its calibration curve. All spectra were measured at room temperature.

2.3 Analysis techniques The measured ER spectra were least-squares fitted with an appropriate sum of several conventional derivative-like functional forms (DLFFs) given by:

$$\frac{\Delta R}{R} = \mathrm{Re}\left[\frac{C\,\mathrm{e}^{i\theta}}{\left(E - E_\mathrm{g} + i\Gamma\right)^n}\right], \tag{2}$$

where E is the photon energy, E_g the transition energy, C an amplitude, θ a phase, and Γ a broadening. The exponent n can be assumed to have several values, with $n = 2$ being appropriate for excitonic lineshapes at low temperatures. Equation (2) is in fact not formally correct for QW excitonic lineshapes at room temperature. However, it has been shown that Eq. (2) with $n = 3$ mimics the correct lineshape [5]. Here, we found that the value chosen for n did not significantly affect either the quality of the fit or the fitted values for E_g and we present results using $n = 2.5$.

SPV signals are essentially approximately proportional to the absorption spectrum of the sample and, in the case of QWs, can yield simple peaks near the excitonic transitions [6]. Such signals can be analysed by several methods [4, 7–9]. Here we adopted the procedure recommended by Ref. [4], whereby the SPV was multiplied by the photon energy and then numerically differentiated to yield $d(E \times \mathrm{SPV})/\mathrm{d}E$. Such a derived spectrum may then also be fitted with Eq. (2), in this case with $n = 2$ [4].

The measured transition energies obtained in this way from the ER and SPV were compared to those predicted by solving the Schrödinger equation for particles in a square-well potential [10]. The material parameters for the various alloys in the structures, including the strained QW bandgap energy E_g, the barrier bandgap E_gB, the associated electron and hole masses, and the conduction band offset Q_c, were taken initially from the tabulated recommended data of Vurgaftman et al. [11]. Here, we define Q_c by $\Delta E_\mathrm{c}/(\Delta E_\mathrm{c} + \Delta E_\mathrm{v,hh})$ where ΔE_c is the depth of the QW conduction band (CB) confinement potential for electrons, and $\Delta E_\mathrm{v,hh}$ the corresponding valence band (VB) confinement potential for heavy holes (hh). In addition, the QW calculations took account of the small red-shift of the transition energies due to the effects of excitonic binding energies (typically ~3 or ~4 meV), according to the description of Mathieu et al. [12, 13].

In order to achieve a match of the predicted QW transition energies with those measured, a special QW Monte Carlo (QWMC) program was written, as described next. This program randomly varied four key parameters; the strained QW bandgap energy E_g, the barrier bandgap E_gB, the CB offset Q_c and the well width L_z, within pre-defined limits, as deemed suitable given the growth tolerances likely for the material system concerned. For each random

choice of these four values, the square-well Schrödinger equation was then solved and the predicted QW transition energies (including excitonic binding energies, and assuming all QWs within a given sample are identical) were compared to the measured ones. The QWMC program was then run for several thousand iterations to search for the four parameter values that gave the closest match to the experimental transition energies. Having obtained this best match, the remaining material parameters, such as effective masses (which have a much smaller effect on the theoretical predictions) were then refined using the QW and barrier material compositions corresponding to these new values of E_g and E_{gB}, again using the tabulated literature data [11]. This process was repeated until it converged on consistent values of E_g, E_{gB}, Q_c and L_z that gave the best match between the theoretical and measured transition energies.

3 Results Figures 1 and 2 compare the ER and SPV spectra for the two tri-metal samples A and B, respectively. In both samples, the SPV and ER spectra exhibit a clear feature from the QW ground state transition near 0.80 eV, and several higher order QW transitions, perhaps most clearly seen as an SPV peak near 0.87 eV in Fig. 1 and a weaker shoulder below this at ~0.84 eV. There are also clear features from the barrier in the SPV and ER spectra near 1.013 eV (see vertical arrow in Fig. 1), with strong above-bandgap Franz–Keldysh oscillations (FKO) in the ER. Both the ER and SPV spectra show additional interference-related oscillations between about 1.1 eV and 1.3 eV. The SPV shows an additional peak near 0.94 eV. Samples A and B have broadly similar spectra, with each of the aforementioned features occurring in similar positions. It is clear that the ER and SPV signal amplitudes of sample B are significantly lower than those of sample A. This difference is believed to be due mainly to the fact that

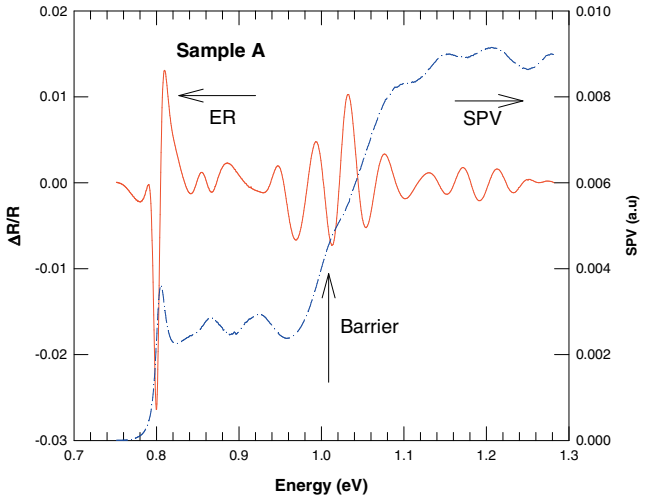

Figure 1 (online colour at: www.pss-a.com) Comparison of the ER (full curve) and SPV (dash-dot curve) of tri-metal sample A. The vertical arrow indicates the barrier bandgap transition feature in the SPV.

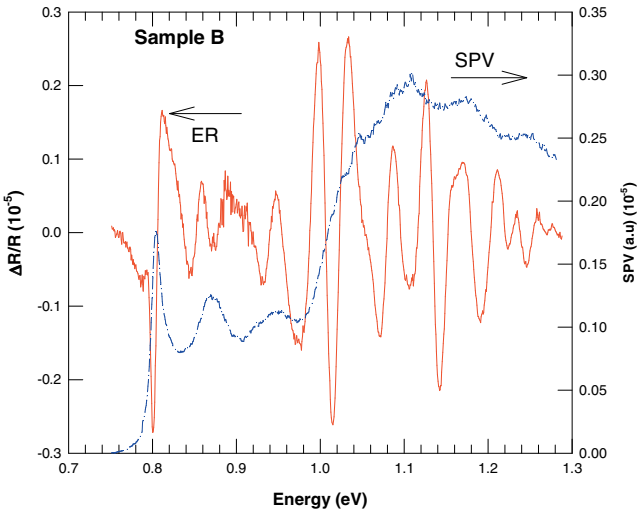

Figure 2 (online colour at: www.pss-a.com) Comparison of the ER (full curve) and SPV (dash-dotted curve) of tri-metal sample B.

the AlInAs blocking layers in sample B are undoped (see Section 2.1) resulting in a weaker built-in electric field. However, slight dissimilarities in the small air gap, and so contact resistance, between the ITO electrode and sample in the soft contact mode technique may also be partly responsible for such differences from sample to sample. There were no other intended differences in the growth of samples A and B.

It is worth noting that we investigated the effect on the ER of changing both the AC voltage amplitude and bias,

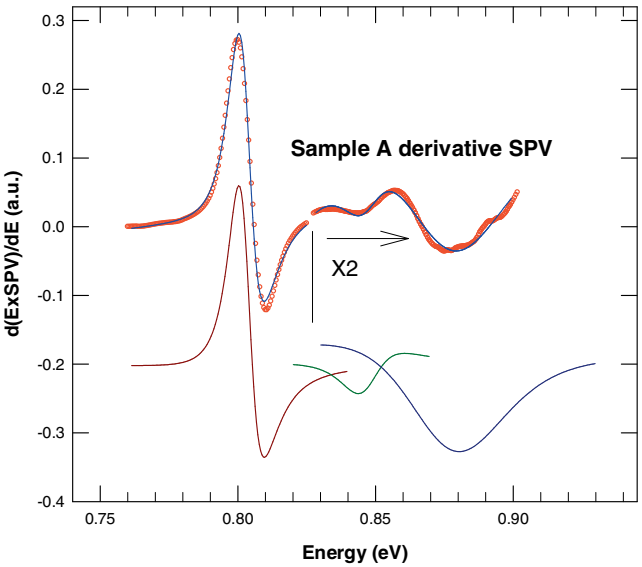

Figure 3 (online colour at: www.pss-a.com) Detail of the derived SPV (small circles) of tri-metal sample A over the energy-region of the confined QW transitions, together with a fit (full curve). Also shown underneath are the three constituent DLFFs. Beyond 0.83 eV, the data, fit and latter two DLFFs have been magnified by two, for clarity.

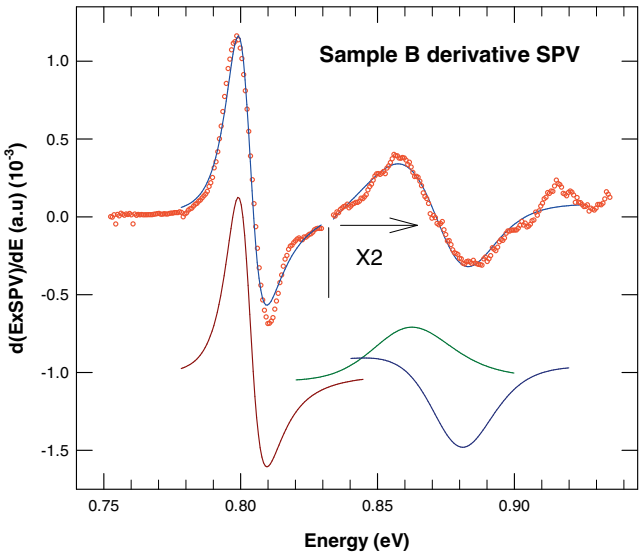

Figure 4 (online colour at: www.pss-a.com) Detail of the derived SPV (small circles) of tri-metal sample B over the energy-region of the confined QW transitions, together with a fit (full curve). Also shown underneath are the three constituent DLFFs. Beyond 0.83 eV, the data, fit and latter two DLFFs have been magnified by two, for clarity.

and found that this mainly affected only the signal amplitude. We also investigated the effects of changing the contact method in the ER: from soft-contact ITO to direct contact silver paste (in the form of an annular electrode, surrounding the illuminated spot). This changed mainly only the phase of the resulting ER spectrum, though there were some other differences, on which we will elaborate later.

The ER spectra and numerically-differentiated SPV spectra of both samples were then fitted with a sum of appropriate expressions like Eq. (2). The fitting to the differential SPV was fairly straightforward using three such terms to describe the observed ground- and two excited-state QW transitions.

Table 1 Fitted experimental and theoretical transition energies of tri-metal sample A, due to the associated QW transitions. The first column shows the results of fitting the ER spectrum. The pair of nearly degenerate energies near 800 meV are explained in the main text. The second column shows the results of fitting the differential SPV spectrum. The third column, labelled 'QWMC' is the final result of the Monte-Carlo process of matching the fitted energies in the first column (ER) with theory. The fourth column indicates the corresponding identity of the QW transition, where, e.g. H_{11} refers to the first confined electron- to first heavy-hole-state transition.

sample A			
expt. (ER) (meV)	expt. (SPV) (meV)	QWMC (meV)	transition
793 ± 5/801 ± 2	803 ± 2	801 ± 1	H_{11}
849 ± 3	847 ± 3	857 ± 1	H_{12}
876 ± 5	876 ± 9	876 ± 1	L_{11}

Table 2 Fitted experimental and theoretical transition energies, as in Table 1, due to the associated QW transitions, only for tri-metal sample B.

sample B			
expt. (ER) (meV)	expt. (SPV) (meV)	QWMC (meV)	transition
802 ± 6/802 ± 2	803 ± 2	802 ± 1	H_{11}
856 ± 3	861 ± 8	857 ± 1	H_{12}
879 ± 4	879 ± 6	876 ± 1	L_{11}

Both samples gave reasonably satisfactory fits, as shown in Figs. 3 and 4, with broadly similar fitted transition energies, as shown collated in Tables 1 and 2.

However, a slight complication was encountered when it came to fitting the corresponding ER spectra: it may be seen from Figs. 1 and 2 that there appears to be a weak additional ER feature near the QW ground-state transition, perhaps most clearly seen as a small trough near 0.78 eV. This proved to be quite troublesome when trying to achieve an acceptable fit to the ER spectra, which could not be accomplished unless an extra weak DLFF was included to account for this feature. When left free to vary in the fits, the energy of this DLFF converged to a value very close to, or slightly below (a few meV at most) the main QW ground-state transition. This extra oscillator, which was always weaker and broader than the main QW ground-state transition, may be seen in the component oscillators displayed in both Figs. 5 and 6. Including it allowed excellent overall fits to be obtained (see Figs. 5 and 6). It may be seen, perhaps most clearly in Fig. 6, that this extra feature not only accounts well for the trough near 0.78 eV, but also for a weak shoulder on the main QW ground-state feature near 0.83 eV, which we take as further corroboration of its undoubted presence in these ER spectra.

The origin of this extra weak ER feature is not clear at this time but it could arise from either a shallow impurity state, or from effects of a non-uniformity of the applied electric field in the sample, such that at least one of the four QWs generates a slightly different-phase ER signal for its ground-state transition. Such an extra feature manifestly has no counterpart in the differential SPV spectra (see Figs. 3 and 4), so the interpretation based on field non-uniformity is more appealing. This is further supported by our observations of the effect of changing the contacting method in the ER, as mentioned earlier, which might well change the field non-uniformity: when the ER of sample A was measured using a direct-contact annular electrode made of silver paste, the trough near 0.78 eV, though still present, became relatively much weaker. Therefore, we believe the most likely interpretation at this time is that this extra feature arises due to field non-uniformities. There is insufficient space here to provide further exposition of

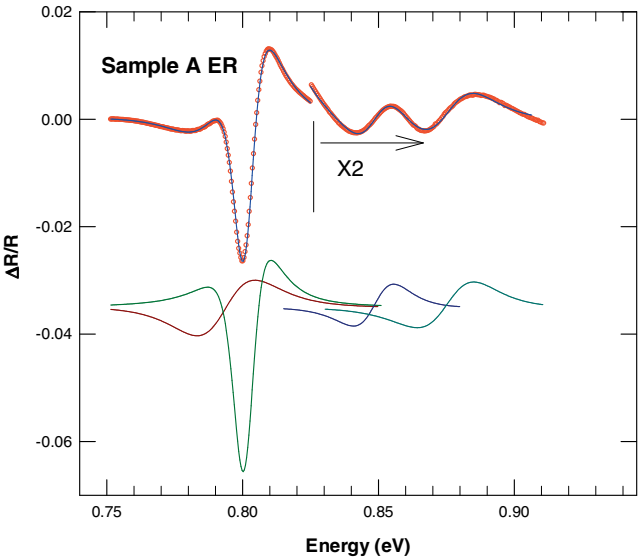

Figure 5 (online colour at: www.pss-a.com) Detail of the ER (small circles) of tri-metal sample A over the energy-region of the confined QW transitions, together with a fit (full curve). Also shown underneath are the four constituent DLFFs. Beyond 0.83 eV, the data, fit and latter two DLFFs have been magnified by two, for clarity.

such effects on ER spectra, and a more detailed systematic study will be published elsewhere.

If a different ER signal occurs from the ground-state transition for at least one QW, then one might expect to observe extra weaker, broader higher-order transitions of this QW in the ER. However, the existing observed higher-order transitions are already quite broad so it is feasible

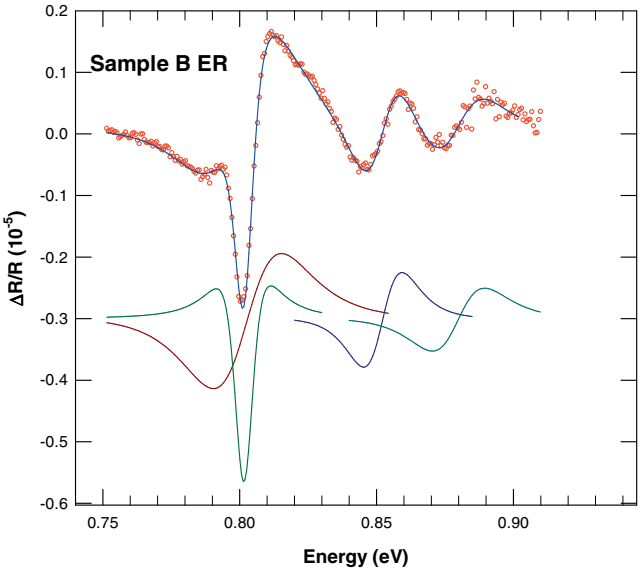

Figure 6 (online colour at: www.pss-a.com) Detail of the ER (small circles) of tri-metal sample B over the energy-region of the confined QW transitions, together with a fit (full curve). Also shown underneath, are the four constituent DLFFs.

that any such extra transitions may be present at the same energies, but masked by their stronger counterparts. Certainly, excellent ER fits were obtainable without having to account for any such possible extra higher-order QW transitions.

As Tables 1 and 2 show, the fitted transition energies of the ER and SPV agree to within ≤~5 meV for a given sample. Comparing samples A and B for either ER or SPV, the three fitted QW transition energies are generally equal to within experimental uncertainty.

For both samples A and B, the three observed QW transition energies from the ER fits were then used in the QWMC program to find the best match with those generated by theory, as described in Section 2.3 (because of the similarity of the ER and SPV results, only the ER values were used for this procedure.) Tables 1 and 2 show that a generally satisfactory match was achieved for both samples A and B. The observed QW features were thus identified as transitions between the single confined electron state and either: first hh state (denoted here as transition H_{11}); second hh state (H_{12}) and; single confined light-hole (lh) state (L_{11}). The QW width needed to obtain the match was 49 ± 0.5 Å, as compared to the target of 45 Å. It is possible that we may also be detecting QW width variations both between the four wells, and also in the lateral direction across our samples, since the size of the illuminated spot in the ER and SPV measurements was ~1 mm × ~2 mm.

The QWMC uncertainties quoted in Tables 1 and 2 come from the fact that the QWMC program would locate a small range of parameter values where the match between the predicted and experimental transition energies was comparable (i.e. within the uncertainties quoted in Tables 1 and 2).

The QW and barrier compositions for samples A and B, were deduced from that which gave the best match in the QWMC program, assuming a 1% strained QW and a lattice-matched barrier. After refining the effective masses, as described in Section 2.3, the best match yielded a strained QW bandgap of 690 ± 1 meV and a barrier bandgap of 1013 ± 1 meV, corresponding to compositions of $In_{0.680}Ga_{0.275}Al_{0.045}As$ and $In_{0.530}Ga_{0.276}Al_{0.194}As$, respectively. The deduced barrier bandgap is slightly off the 992 meV target mentioned in Section 2.1 but the SPV, and its differential, clearly show the barrier feature is indeed located close to 1013 meV (see Fig. 1). The CB offsets required to achieve the best match were found to be 66 ± 1% for both samples A and B, as compared to a value of ~63% that would be expected for the above compositions using the literature data [11].

As mentioned earlier, it can be seen in the SPV of Figs. 1 and 2, that there is possibly at least one other feature near 940 ± 15 meV in samples A and B. However, the close proximity of these features to the strong barrier signal (with additional FKO in the case of the ER – see Figs. 1 and 2) made it impossible to perform reliable least-squares fits in this region to obtain any transition energies. Furthermore, such energies lie beyond any calculated con-

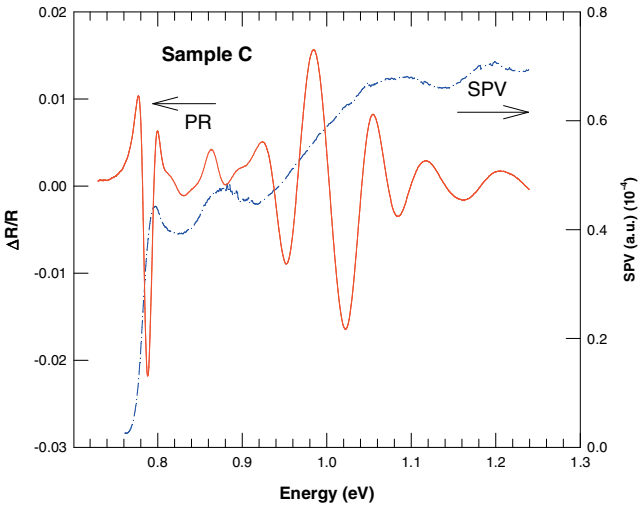

Figure 7 (online colour at: www.pss-a.com) Comparison of the PR (full curve) and SPV (dash-dot curve) of benchmark InGaAsP sample C.

fined-state transitions. However, the QW program predicted that several across-interface transitions may occur at such high energies, such as from the barrier VB to the confined electron state (at ~892 meV), or from the two hh confined states to the barrier CB (at ~926 meV and ~982 meV, respectively). It is believed that the observed high-energy feature(s) could arise from a combination of such across-interface transitions. It is also worth noting that the two 1000 Å InGaAlAs graded-index regions (see Section 2.1), may generate additional spectral contributions over the ~990 meV to ~1180 meV energy range.

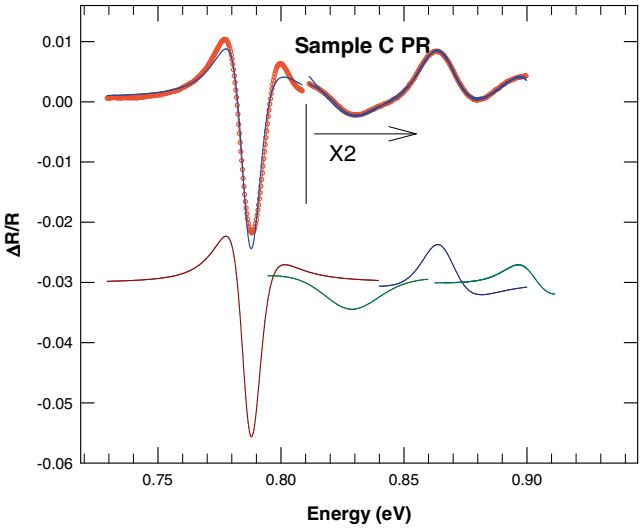

Figure 8 (online colour at: www.pss-a.com) Detail of the PR (small circles) of benchmark InGaAsP sample C over the energy-region of the confined QW transitions, together with a fit (full curve). Also shown underneath are the four constituent DLFFs. Beyond 0.81 eV, the data, fit and latter three DLFFs have been magnified by two, for clarity.

A similar analysis was performed for the InGaAsP benchmark sample. In this sample only, a strong PR signal was measurable (using the HeNe laser), in addition to a similar ER $\Delta R/R$ signal, which was, however, about 20 times weaker. In Figs. 7 and 8, we choose to show the PR spectrum, together with the SPV. We observe four distinct QW transitions, with fitted energies given in Table 3. Unfortunately, in this sample the differential SPV clearly revealed only the ground state transition, with a fit giving ~784 meV, in fair agreement with the fitted PR result of 787 meV (see Fig. 7). Table 3 also gives the final results of the QWMC simulation showing that, in addition to H_{11}, H_{12} and L_{11}, the H_{13} transition between the single confined electron state and third confined hh state is also predicted and observed in this sample. The match shown in Table 3 was obtained with a Q_c of 39 ± 3%, which is reasonably close to that expected (~34%) for this structure's composition [11]. As expected, this CB offset is significantly lower than the ~66% found for the tri-metal samples, showing that the electrons are indeed more poorly confined in this system.

The QWMC result for sample C for L_z was 60 ± 1 Å, close to the nominal 65 Å. For the QW and barrier bandgaps, the best match occurred with E_g = 715 ± 6 meV and E_{gB} = 994 ± 12 meV, respectively. Though the latter agrees well with the target barrier bandgap of ~992 meV, the result for the strained QW bandgap E_g is somewhat lower than would be expected (~770 meV) given the nominal QW composition of Section 2.1 [11]. However, this is perhaps unsurprising, since the measured QW ground-state transition at ~787 meV in sample C corresponds to a wavelength of 1.58 μm, somewhat above 1.55 μm. We note that band-filling effects under laser operation may shift the emission wavelength closer to 1.55 μm. Furthermore, in the actual devices the exact operation wavelength is tightly controlled using a distributed feedback structure.

Figure 9 compares the band alignment schematics for the tri-metal and benchmark samples, based on the final matches achieved with experiment using the QWMC program. This shows quite clearly the effect of using a tri-metal alloy instead of the usual InGaAsP quaternary, in particular on the electron confinement potential: while in the tri-metal samples the electron well has a depth of ~218 meV, it is only ~110 meV in the benchmark sample.

Table 3 Fitted experimental and theoretical transition energies, as in Table 1, only for benchmark InGaAsP sample C.

sample C		
expt. (PR) (meV)	QWMC (meV)	transition
787 ± 2	780 ± 3	H_{11}
827 ± 6	828 ± 2	H_{12}
866 ± 4	877 ± 2	L_{11}
902 ± 4	901 ± 2	H_{13}

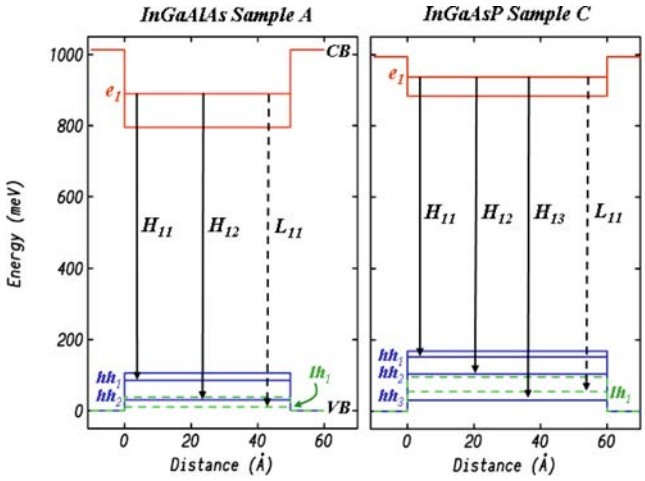

Figure 9 (online colour at: www.pss-a.com) Schematic of band alignments resulting from QWMC calculations (see Tables 1 and 3) for InGaAlAs sample A and InGaAsP sample C, showing electron (e) and heavy-hole (hh), conduction and valence bands (CB and VB, respectively) in the barrier and QW, together with confined electron and hole energy-levels (solid horizontal lines). The dashed lines show the corresponding results for the light holes (lh). As may be seen, the electron QW is deeper in the tri-metal sample A, as intended, corresponding to a CB offset of ~66%, in contrast to the ~40% of sample C. The observed transitions are shown by the vertical arrows, whose lengths are equal to the transition energies (not including the slight red-shifts due to excitonic binding energies.)

On the other hand, the holes are less strongly confined in the InGaAlAs samples with hh and lh well depths of ~105 meV and ~38 meV, respectively, compared to corresponding depths of ~169 meV and ~96 meV, respectively, in the InGaAsP wells. The combination of an increased CB offset, which reduces electron spill-over, coupled with the low VB offset, which reduces the QW hole density, both serve to reduce non-radiative loss processes such as Auger recombination in the InGaAlAs system, as has been reported elsewhere [14].

4 Summary and conclusions Modulated reflectance and surface photovoltage spectra have been measured at room temperature for two tri-metal InGaAlAs QW laser structures and compared to those of a benchmark InGaAsP QW structure, all designed to lase at 1.55 μm. The tri-metal samples were found to exhibit three confined-state QW transitions, whereas the InGaAsP sample showed a fourth, due to the more deeply-confined heavy holes in this structure. The SPV spectra generally corroborated the measured QW transition energies obtained in the ER or PR. The experimentally-determined transition energies were matched to those theoretically predicted by the Schrödinger equation, in which four key parameters (the strained QW bandgap energy, the barrier bandgap, the CB offset and the well width) were varied using a Monte-Carlo technique.

In the tri-metal samples, a close match was obtained between the theoretical and experimental transition energies. The resulting deduced barrier and QW bandgaps yielded the likely material compositions. The calculations also confirmed that both samples have a well width within ~5 Å of the target 45 Å. The best match CB offset was Q_c ~66%, which lies close to the ~63% expected using literature data [11], confirming that the electrons are indeed strongly confined in this system.

In the InGaAsP benchmark sample, the ground-state QW transition wavelength was found to be at ~1.58 μm. While the fit to the spectra yielded QW transition energies that were consistent with more poorly confined electrons, as expected (with a Q_c of ~40%), their energy positions confirmed that the QW had a somewhat smaller bandgap energy than nominally expected, possibly due to a slight compositional growth variations, though the fitted average well-width was again within ~5 Å of the target 65 Å.

The tri-metal laser structures have been clearly demonstrated to have a higher CB offset than the more conventional InGaAsP QW structures. Consequently, the electron confinement potential in the InGaAlAs wells is about twice as deep as that in the InGaAsP system. This confirms that these tri-metal QW laser structures will benefit from having a larger potential wavelength range and improved thermal performance.

Acknowledgements We would like to thank Dr. Stuart Cripps for kindly providing his program that generated the material parameters according to the recommended tabulated data of Vurgaftman et al. [11]. We also acknowledge the British Council, New Delhi, for providing financial support for TKS under the UKIERI fellowship, the EPSRC for providing a Ph.D. studentship for NEF, and to Bookham for providing the samples as part of the TSB (UK) supported "ETOE" programme.

References

[1] N. Imoto et al., J. Quantum Electron. **16**(10), 1053–1056 (1980).
[2] D. Olego et al., Appl. Phys. Lett. **41**(5), 476–478 (1982).
[3] S. Datta et al., Rev. Sci. Instrum. **72**(1), 177–183 (2000).
[4] B. M. Arora et al., Mater. Sci. Semicond. Process. **4**, 489–495 (2001).
[5] B. V. Shanabrook et al., Phys. Rev. B **35**, 2540 (1987).
[6] Ts. Ivanova et al., J. Appl. Phys. **101**, 114309 (2007).
[7] B. Čechavičius et al., J. Appl. Phys. **98**, 023508 (2005).
[8] C. H. Chan et al., J. Appl. Phys. **103**, 084303 (2008).
[9] J. S. Liang et al., Appl. Phys. Lett. **79**(20), 3227–3229 (2001).
[10] M. Scharff, Elementary Quantum Mechanics (John Wiley & Sons, 1969), p. 58.
[11] I. Vurgaftman et al., J. Appl. Phys. **89**(11), 5815–5861 (2001).
[12] H. Matthieu et al., J. Appl. Phys. **72**(1), 300–302 (1992).
[13] H. Matthieu et al., Phys Rev. B **46**(7), 476–478 (1992).
[14] S. J. Sweeney et al., Phys. Status Solidi B **241**, 3391–3398 (2004).

